JOURNAL OF GEOPHYSICAL RESEARCH, VOL. 115, B07403, doi:10.1029/2009JB006967, 2010

Combination of geodetic observations and models for glacial isostatic adjustment fields in Fennoscandia

Emma M. Hill,[1] James L. Davis,[1] Mark E. Tamisiea,[2] and Martin Lidberg[3,4]

Received 9 September 2009; revised 15 January 2010; accepted 17 February 2010; published 13 July 2010.

[1] We demonstrate a new technique for using geodetic data to update a priori predictions for Glacial Isostatic Adjustment (GIA) in the Fennoscandia region. Global Positioning System (GPS), tide gauge, and Gravity Recovery and Climate Experiment (GRACE) gravity rates are assimilated into our model. The technique allows us to investigate the individual contributions from these data sets to the output GIA model in a self-consistent manner. Another benefit of the technique is that we are able to estimate uncertainties for the output model. These are reduced with each data set assimilated. Any uncertainties in the GPS reference frame are absorbed by reference frame adjustments that are estimated as part of the assimilation. Our updated model shows a spatial pattern and magnitude of peak uplift that is consistent with previous models, but our location of peak uplift is slightly to the east of many of these. We also simultaneously estimate a spatially averaged rate of local sea level rise. This regional rate (~1.5 mm/yr) is consistent for all solutions, regardless of which data sets are assimilated or the magnitude of a priori GPS reference frame constraints. However, this is only the case if a uniform regional gravity rate, probably representing errors in, or unmodeled contributions to, the low-degree harmonic terms from GRACE, is also estimated for the assimilated GRACE data. Our estimated sea level rate is consistent with estimates obtained using a more traditional approach of direct "correction" using collocated GPS and tide gauge sites.

Citation: Hill, E. M., J. L. Davis, M. E. Tamisiea, and M. Lidberg (2010), Combination of geodetic observations and models for glacial isostatic adjustment fields in Fennoscandia, *J. Geophys. Res.*, *115*, B07403, doi:10.1029/2009JB006967.

1. Introduction

[2] Glacial isostatic adjustment (GIA) is the ongoing viscoelastic deformation of the Earth and adjustment of the oceans in response to the loading and unloading of the ice sheets associated with the glacial cycles. The present-day GIA signature is dominated by the rapid melting of the ice sheets associated with the last glacial maximum occurring ~22,000 years ago. A large literature is devoted to the numerical prediction of GIA. Assuming a spherically symmetric Earth structure, viscoelastic loading Green's functions [e.g., *Peltier*, 1974] are calculated using an Earth model that describes the viscoelastic structure of the lithosphere and mantle. The viscoelastic Green's functions are convolved with a model for the time-dependent glacial load. The self-gravitation and loading effects associated with redistribution of the glacial meltwater in the oceans are accounted for by solving the sea level equation [e.g., *Farrell and Clark*, 1976; *Clark et al.*, 1978; *Mitrovica and Peltier*, 1991]. Recently, a number of additional features have been included, such as the altered geometry of the ocean load with changing sea level and variations in marine-based ice [*Johnston*, 1993; *Peltier*, 1994, 1998; *Milne et al.*, 1999; *Mitrovica and Milne*, 2003], as well as the "feedback" effect on Earth rotation [*Han and Wahr*, 1989; *Bills and James*, 1996; *Milne and Mitrovica*, 1996; *Mitrovica et al.*, 2005]. More recently, GIA modelers have begun experimenting with more realistic, nonsymmetric Earth models [*Tromp and Mitrovica*, 2000; *Martinec*, 2000; *Wu*, 2004; *Latychev et al.*, 2005; *Paulson et al.*, 2005].

[3] Numerical predictions of GIA are therefore sensitive to errors in the adopted Earth and ice history model, and to modeling assumptions and simplifications. Using observations to constrain the models necessarily includes further simplifications required to reduce the solution to a tractable problem. A common approach, for example, is to assume that the ice history model is correct, and to use a data set to estimate corrections to the Earth model (generally mantle viscosity and effective lithospheric thickness) for a limited number of spherical layers. This approach yields an Earth-ice model combination in which neither component of the combination is necessarily correct, but which fits the observations at some level. Although this is a reasonable approach in many cases, where the trade-offs between ice history and Earth models are minimal (especially the case in previously glaciated areas) [e.g., *Wahr and Davis*, 2002],

[1]Harvard-Smithsonian Center for Astrophysics, Cambridge, Massachusetts, USA.
[2]National Oceanography Centre, Liverpool, UK.
[3]Onsala Space Observatory, Chalmers University of Technology, Gothenburg, Sweden.
[4]Now at Geodesy Division, Lantmäteriet, Gävle, Sweden.

0148-0227/10/2009JB006967

some data sets exhibit trade-offs between these models [e.g., *Sabadini and Vermeersen*, 2004], and the GIA model parameter estimation approach inevitably leads to systematic errors.

[4] The need for a new approach is acute now that there are modern space-geodetic regional data sets of high accuracy acquired within previously glaciated areas. One such example is Fennoscandia, which has an extremely rich data set for measuring GIA following late-Pleistocene glaciation in the region.

[5] For example, the BIFROST (Baseline Inferences for Rebound Observations, Sea level, and Tectonics) Project includes a network of continuously operating Global Positioning System (GPS) sites across Fennoscandia, some of which have been operating since 1993, that have been used to determine the three-dimensional deformation due to GIA in this area. *Milne et al.* [2001], *Johansson et al.* [2002], and *Milne et al.* [2004], compared initial results from this network to numerical models for GIA. All these studies found generally good agreement between the GPS results and GIA models, but also some significant differences. (The models were tuned to fit the data, so general agreement is not surprising.) The magnitude of maximum uplift (10–11 mm/yr) was similar for both models and data. However, the geographic distributions were slightly different, causing some significant residual rates in both the horizontal and radial components (e.g., RMS residuals for observations minus model, in the radial component, were 1.3 mm/yr [*Johansson et al.*, 2002]). These differences were suggested to be due to inaccuracies or simplifications in the Earth or ice model used for the GIA calculations, although systematic errors in the GPS results are also discussed. *Lidberg et al.* [2007] later updated the BIFROST GPS solutions with a longer time series and a different processing technique. They compared their results to both the previous GPS solution from *Johansson et al.* [2002] and the model for GIA computed by *Milne et al.* [2001]. Again there was generally good agreement between observations and models, but *Lidberg et al.* [2007] found small biases between their solution and the previous studies (RMS residuals of ~1 mm/yr). They suggested that the biases could be the result of differences in the reference frame realization. As with the previous studies, *Lidberg et al.* [2007] found maximum discrepancies between their results and the GIA models in the north of Fennoscandia.

[6] The Fennoscandia GIA signal can also be observed in time-dependent gravity rates determined by the NASA GRACE (Gravity Recovery And Climate Experiment) mission. *Steffen et al.* [2008] present GRACE results for the Fennoscandia region from ~5 years of data. In comparing their GRACE results with a GIA model they found good agreement between the magnitude and location of peak uplift (maximum of 1.33 μGal/yr for the model, 1.2 μGal/yr for the GRACE results), but inconsistencies in the geographical extent of the uplift signal.

[7] Additionally, the tide gauge network around Fennoscandia and the Baltic Sea is one of the longest running and most densely spaced in the world, with many stations in continuous operation since the late 19th century. Measurements of relative sea level change from this network have been made available by the Permanent Service for Mean Sea Level (PSMSL) [*Woodworth and Player*, 2003]. Data from this network have not generally been used for estimates of global eustatic sea level change due to the difficulty in removing the GIA signal from the records of relative sea level change. However, previous studies [*Davis et al.*, 1999; *Kuo et al.*, 2004] have demonstrated the utility of the tide gauge data to studying the GIA signal itself. *Kuo et al.* [2004] compared estimates of land uplift from a combination of TOPEX/Poseidon and tide gauge data with rates from 10 BIFROST GPS sites and found good agreement. They found larger discrepancies between their results and those from numerical models.

[8] As indicated, previous studies have examined the GPS, GRACE, and tide gauge data sets individually, showing general agreement with each other and with numerical models, but with some inconsistencies. Some of these inconsistencies may be due to difficulties in comparing results from different models and data in a self-consistent way. Each individual data type is subject to particular systematic errors, has particular spatial sampling and resolution, and may be sensitive to additional, non-GIA effects. (For example, tide gauge data measure the changing sea surface relative to the solid Earth. Both of these are affected by GIA, but the sea surface rate is additionally modified by present-day ocean volume, steric, and atmospheric changes.) Due to these different errors, resolutions, and sensitivities, the different data types therefore represent a somewhat inconsistent picture of the GIA process.

[9] In this paper, we make use of an approach that may be considered consistent with both the least squares collocation technique [*Moritz*, 1980] and data assimilation [e.g., *Bennett*, 2002]. This method enables us to combine the different data types and spatial sampling to solve for GIA fields (gravity, deformation, and sea level) on a regular grid. This approach has not been used before to estimate GIA because the GIA theory is so complex, resulting in relationships between the GIA field types (gravity, deformation, sea level) that are difficult to represent. In our approach, these relationships are expressed as covariances, which we calculate as sample covariances using a suite of values from GIA code based on the theoretical improvements collected by *Mitrovica and Milne* [2003] and *Kendall et al.* [2005]. Using this approach we combine the geodetic data into an a priori GIA model to produce a new and updated model for GIA. We have several goals: (1) to produce an updated GIA field that is less dependent on knowledge of the ice history or Earth model, for uses such as correction of the geodetic measurements; (2) to investigate the various contributions of the different data sets to the final GIA model and examine biases between these data sets in a self-consistent manner; and (3) to examine whether we can simultaneously estimate a robust and self-consistent estimate of spatially averaged local sea level rise within our assimilation code. This technique was also used to produce the GIA model for the Stable North America Reference Frame (SNARF) (available at http://www.unavco.org/research_science/workinggroups_projects/snarf/snarf.html). We begin by describing the approach.

2. Approach

[10] We let u be a vector of parameters representing the unknown components of the GIA field to be estimated. We use the term "GIA field" to represent any type of GIA-

related observables, such as present-day three-dimensional crustal deformation rates, present-day gravity rates, or present-day relative sea level rates. (We will confine ourselves to these field types, although there could be others.) The parameter vector u may contain multiple GIA observation types. We typically wish to estimate these parameters on an evenly spaced grid of locations. We also have a vector of GIA-field observations d, not necessarily obtained on a grid. The vector u contains the GIA-field values corresponding to the union of the grid locations and the locations for which we have observations. We seek a solution $u = \hat{u}$ that minimizes the penalty function J [e.g., *Bennett*, 2002]

$$J[u] = (d - A \cdot u)^T W^{-1} (d - A \cdot u) + (m - u)^T \Lambda^{-1} (m - u) \quad (1)$$

where m is a vector of prior GIA-field model predictions, the matrices W and Λ are inverse weight (i.e., covariance) matrices associated with the observations and the a priori predictions, respectively, and the design matrix A contains the partial derivatives of the observed values with respect to the parameters

$$A_{ij} = \left.\frac{\partial d_i}{\partial u_j}\right|_{u=m} \qquad i = 1, \ldots, N \quad j = 1, \ldots, M \quad (2)$$

where N is the length of the observation vector and M is the length of the parameter vector. The structure of the design matrix is discussed below. In addition to the GIA-field values, u may contain additional parameters that account for non-GIA effects, such as parameters to account for the GPS reference frame (which may be different to the implicit GIA reference frame) or parameters to account for sea level change not associated with GIA. Equations (1) and (2) implicitly assume that the problem is linear, that the deviations of the solution from both the prior model and the data are small enough that the problem is within the linear regime, or that the problem has been linearized.

[11] In equation (1), the first term of the penalty function represents misfit of the data d with respect to the predicted values for the data based on u, and the second term represents the misfit between the solution and the prior model. Minimization of the penalty function balances these two contributions to the penalty. The elements and structure of W and Λ weight the contributions.

[12] The dimension N of the observation vector must account for all the GIA observations at whatever locations the observations were acquired. For example, if there are n_{GPS} GPS sites then the number of observations might be $N = 3n_{\mathrm{GPS}}$, where the factor of three comes from the three components of velocity. Continuing with the example, if we wish to estimate the three-dimensional GIA deformation at n_{grid} grid points, and to include six reference frame parameters (three rotation, three translation), then the total number of parameters to be estimated is $M = 3n_{\mathrm{GPS}} + 3n_{\mathrm{grid}} + 6$. Clearly, then, the minimization problem has the potential of being highly underconstrained. We overcome this problem by an appropriate choice for the inverse-weight matrix Λ such that the physics of the GIA problem is inherent in the weight matrix. This choice removes many degrees of freedom from the problem.

[13] A straightforward choice for the observational inverse-weight matrix W is the error covariance matrix for the observations. In practice, this will often be a diagonal matrix, although if so-called "loose" GPS solutions (solutions not yet fixed to a terrestrial reference frame) are used the matrix will not be diagonal. (Once a reference frame is established for GPS solutions, nondiagonal elements are so small that the matrix can be treated in practice as if it were diagonal.) The prior GIA predictions, however, are not statistical in nature, as they are derived from forward calculations using adopted Earth and ice history models. Nevertheless, it is possible to calculate the effect of variations of Earth and ice models and propagate those variations into the solution. If Ω represents a set of "reasonable" models, and $\langle m \rangle$ represents the average of the GIA predictions using the N_Ω models in Ω, then an effective model covariance matrix can be calculated:

$$\Lambda_{ij} = \frac{1}{N_\Omega} \sum_{k=1}^{N_\Omega} \left(m_i^k - \langle m \rangle_i\right)\left(m_j^k - \langle m \rangle_j\right) \quad i, j = 1, \ldots, M_{\mathrm{obs}} + M_{\mathrm{grid}} \quad (3)$$

where M_{obs} is the total number of observations ($3n_{\mathrm{GPS}}$ in the previous example), M_{grid} is the number of parameters to be estimated at grid locations ($3n_{\mathrm{grid}}$ in the example), and the superscript k indicates that the GIA predictions were calculated using the kth Earth/ice model combination. Equation (3), though, defines only part of Λ since the dimension of Λ is $M \times M$, where $M = M_{\mathrm{obs}} + M_{\mathrm{grid}} + M_{\mathrm{other}}$, with M_{other} being the number of additional parameters that describe effects that are unrelated to GIA (as discussed above). The covariance of these non-GIA parameters are assumed to be uncorrelated with the model values.

[14] The structure of the design matrix A is straightforward. For $j \le M_{\mathrm{obs}} + M_{\mathrm{grid}}$, the value of A_{ij} of equation (2) will be unity if both the location and GIA field type associated with the indices i and j are the same, and zero otherwise. For index $j > M_{\mathrm{obs}} + M_{\mathrm{grid}}$, A_{ij} is the partial derivative of the observable with respect to an additional, non-GIA parameter.

[15] Each individual term in the penalty function of equation (1) has now been defined. Minimization of the penalty function involves balancing deviations of the parameter solution $\hat{u}$ with respect to observations d against deviations of the solution from the prior model m. The relative weight given to each of these terms is defined by the inverse weight matrices W and Λ. Off-diagonal elements of Λ constrain the deviations among the parameters to physically realistic GIA solutions (i.e., the solution is constrained to fall within a range of values that can be explained by the physics contained in our suite of forward model predictions). In section 2.1, we discuss how the minimization is implemented.

2.1. Implementation

[16] Minimizing the penalty function J of equation (1) with respect to u leads to the solution

$$u = m + \left(A^T W^{-1} A + \Lambda^{-1}\right)^{-1} A^T W^{-1} (d - Am) \quad (4)$$

with covariance matrix

$$\Gamma_u = \left(A^T W^{-1} A + \Lambda^{-1}\right)^{-1} \quad (5)$$

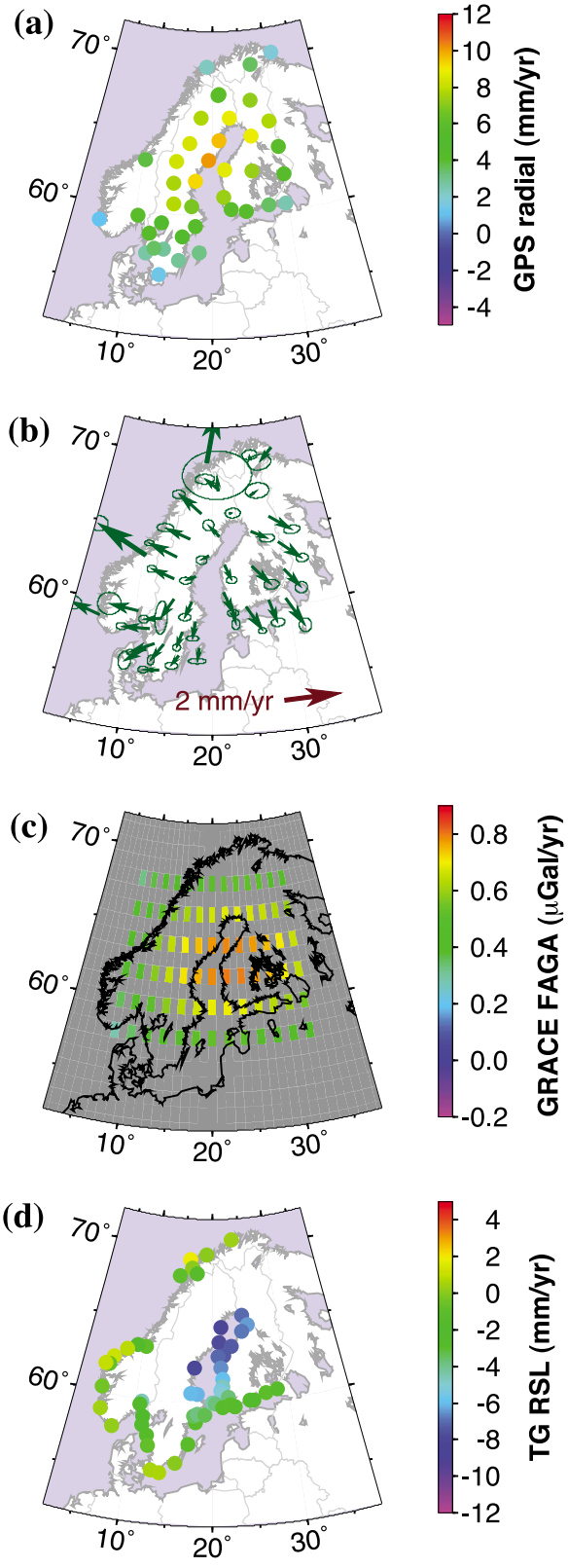

Figure 1. Input geodetic rates: (a) GPS radial deformation, (b) GPS horizontal, (c) GRACE gravity anomaly (minus GLDAS hydrology model), and (d) tide gauge RSL.

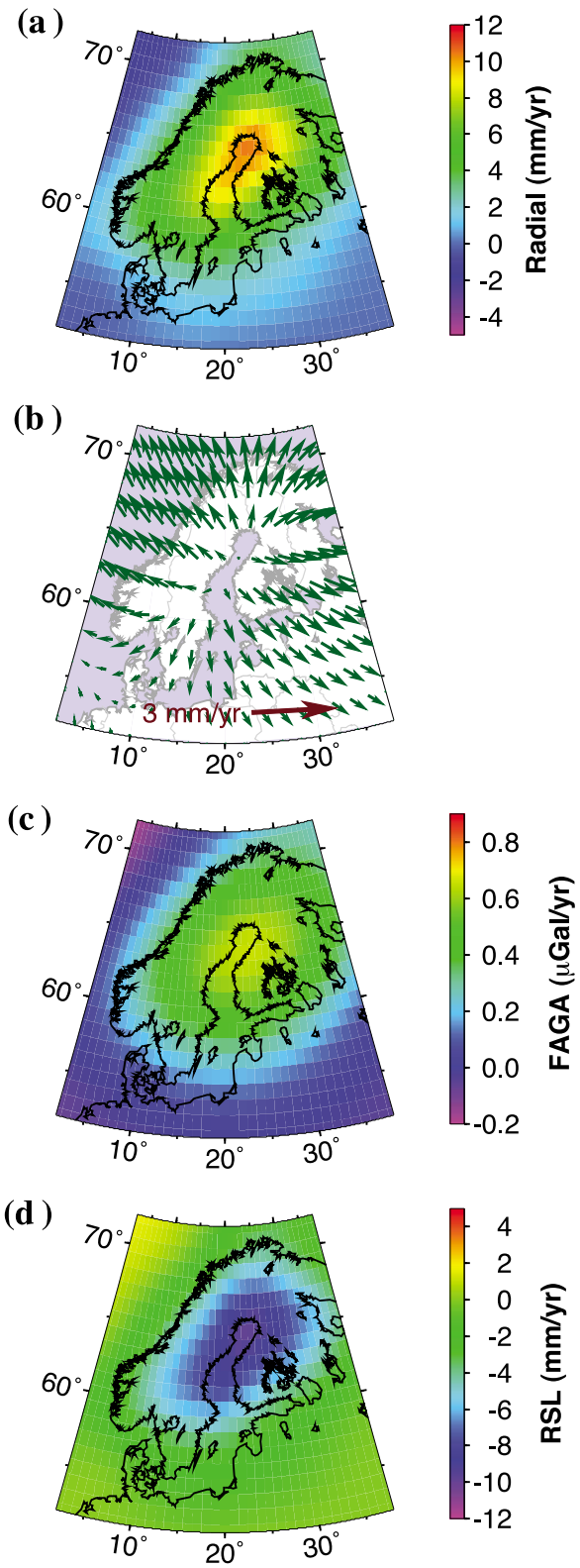

Figure 2. A priori GIA predictions: (a) radial deformation, (b) horizontal deformation, (c) FAGA, and (d) RSL.

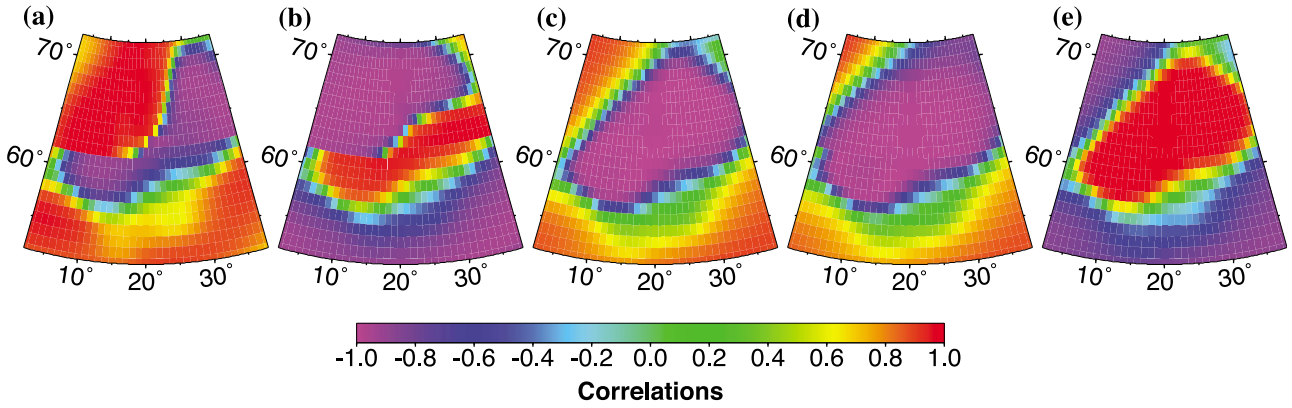

Figure 3. Example correlation plots, all relative to the RSL parameter and a point in the center of the figure (coordinates 20°W, 62°N): (a) East deformation, (b) North deformation, (c) Radial deformation, (d) FAGA, and (e) RSL.

Equations (4) and (5) take the form of a least squares solution with prior constraints. This expression involves two inversions of matrices of order $M \times M$. Depending on the grid size, it is conceivable that the number of grid locations can exceed 1500, and if we estimate three-dimensional deformation and gravity the number of parameters M can therefore exceed 6000. While performing inversions of such matrices is possible, we have chosen to implement a more efficient method.

[17] The first step is to observe that since, under our assumptions, the data are uncorrelated, the solution (equation (4)) can be arrived at iteratively, using the sequential least squares process [e.g., *Xu*, 2003]. In this case, the observation vector d is fed iteratively, one element at a time, into the solution. The ith iteration yields

$$u_i = u_{i-1} + K_i(d_i - A_i u_{i-1}) \tag{6}$$

$$\Gamma_i = \left(A_i^T R_i^{-1} A_i + \Gamma_{i-1}^{-1}\right)^{-1} \tag{7}$$

$$K_i = \Gamma_{i-1} A_i^T R_i^{-1} \tag{8}$$

where $i = 1,\ldots, N$, d_i is the ith element of d, A_i is the ith row of the design matrix, and R_i is the ith diagonal element of W. (In our implementation R_i is a 1×1 matrix.) The initial ($i = 0$) values are $u_0 = m = \langle m \rangle$ and $\Gamma_0 = \Lambda$.

[18] The sequence (6)–(8) still involves multiple inversions of very large matrices, so we make use of well-known matrix identities (Appendix A) to rewrite the expression for K_i and Γ_i in the equivalent forms

$$\Gamma_i = \Gamma_{i-1} - K_i A_i \Gamma_{i-1} \tag{9}$$

$$K_i = \Gamma_{i-1} A_i^T \left(A_i \Gamma_{i-1} A_i^T + R_i\right)^{-1} \tag{10}$$

The expressions (9) and (10) involve somewhat more multiplications, but the only inversions involve a 1×1 matrix. (These equations take the form of a Kalman filter with no dynamics.) Equations (6), (9), and (10) are an efficient formulation for the sequential least squares solution to the minimization of equation (1).

2.2. Observation Equations

[19] In this section we present the observation equations for the three data types used in this study: three-dimensional crustal deformation from GPS, free air gravity anomaly rates from GRACE, and relative sea level rates from tide gauges. We describe these data types further in section 3.

[20] The observation equation for the GPS rates is

$$\dot{\vec{r}}_{GPS}(\lambda, \phi) = \dot{\vec{r}}_{GIA}(\lambda, \phi) + \vec{\Omega} \times \hat{r} + \delta\vec{T} + \vec{\varepsilon}_{GPS}(\lambda, \phi) \tag{11}$$

where $\dot{\vec{r}}_{GPS}(\lambda, \phi)$ is the three-dimensional GPS velocity vector, $\vec{r}_{GIA}(\lambda, \phi)$ is the deformation vector due to GIA, Ω and δT are rotation and translation rate parameters that represent contributions associated with reference frame assumptions, $\hat{r}$ is the site position unit vector, and $\vec{\varepsilon}_{GPS}(\lambda, \phi)$ is a vector of the error. As discussed in section 3, the GPS velocities are determined in a Eurasia-fixed reference frame. However, such a frame is realized either with a particular GIA model or, quite often, with no GIA model. The reference frame parameters thus account for the difference between a Eurasia-fixed reference frame that accounts for the "final" GIA deformation field and the GIA model used in the realization of the Eurasia-fixed reference frame.

[21] For the GRACE data, we choose to use estimates of the free-air gravity anomaly (FAGA), which emphasizes higher-degree variations. The observation equation is therefore

$$\dot{G}_{GRACE}(\lambda, \phi) = \dot{G}_{GIA}(\lambda, \phi) + \varepsilon_{GRACE}(\lambda, \phi) \tag{12}$$

where $\dot{G}_{GRACE}(\lambda, \phi)$ is FAGA rate from GRACE, $\dot{G}_{GIA}(\lambda, \phi)$ is FAGA rate due to GIA, and $\varepsilon_{GRACE}(\lambda, \phi)$ is the error.

[22] The observation equation for the tide gauge rates is

$$\dot{S}_{TG}(\lambda, \phi) = \dot{S}_{GIA}(\lambda, \phi) + \dot{\mu} + \varepsilon_{TG}(\lambda, \phi) \tag{13}$$

where $\dot{S}_{TG}(\lambda, \phi)$ represents the rate of relative sea level (RSL) change from a tide gauge at coordinates (λ, ϕ), $\dot{S}_{GIA}(\lambda, \phi)$ represents model RSL change due to GIA at this location, $\dot{\mu}$ represents a spatially averaged local sea level rate for all tide gauge locations, and $\varepsilon_{TG}(\lambda, \phi)$ is the error. Sea level rise due to present-day melting will not be spatially constant around the globe [e.g., *Mitrovica et al.*, 2001;

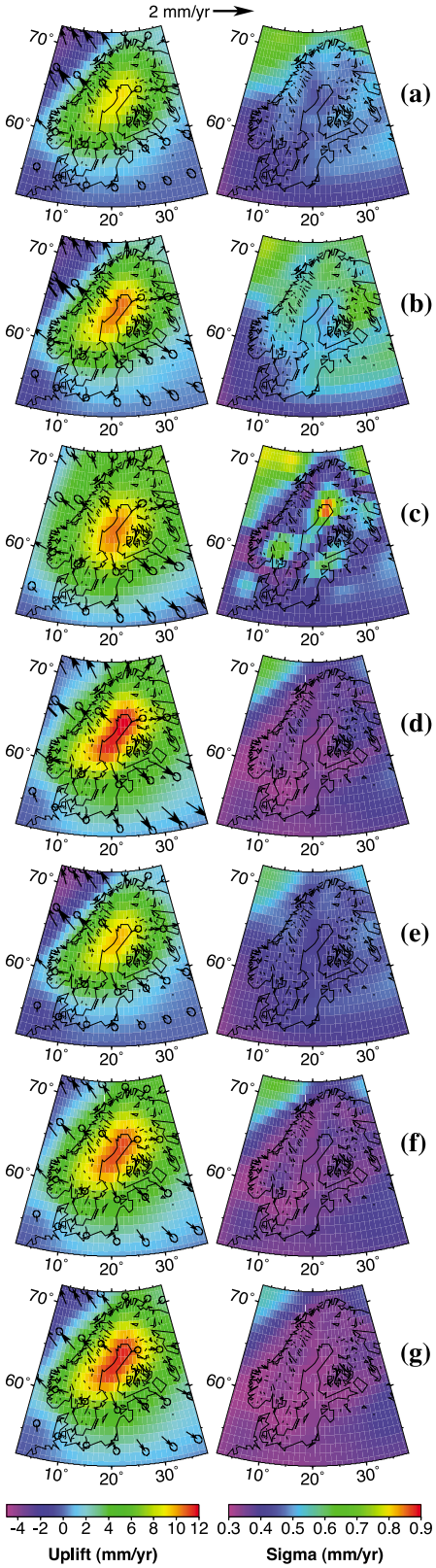

Figure 4. Output GIA models for horizontal and radial deformation, and corresponding uncertainties, with different combinations of geodetic data set assimilated: (a) GPS only; (b) tide gauge only; (c) GRACE only; (d) tide gauge and GRACE; (e) GPS and tide gauge; (f) GPS and GRACE; and (g) GPS, tide gauge, and GRACE.

Tamisiea et al., 2001] but here we ignore these effects over Fennoscandia.

3. Data and Model Inputs

[23] Our technique assimilates estimated rates from GPS, GRACE, and tide gauges into a priori predictions for GIA. The a priori estimates are the average of multiple forward models for GIA. The physics of the GIA are contained in the input covariance matrix.

3.1. GPS Data

[24] We used both radial and horizontal GPS velocities (Figures 1a and 1b) estimated by *Lidberg et al.* [2007]. These are based on ~8.5 years of data (January 1996 to June 2004) from continuous GPS stations in the BIFROST network. We used a subset of 40 of the sites presented by *Lidberg et al.* [2007] as we excluded sites south of the Baltic Sea. This area is likely to be undergoing other forms of deformation unrelated to GIA (e.g., tectonic deformation from Africa-Eurasia plate convergence [*Marotta et al.*, 2004]), and the monument geology is generally of glacial deposits (as compared to bedrock outcrops further north), which limits monument stability.

[25] *Lidberg et al.* [2007] processed the GPS data using the GAMIT/GLOBK software. A network of carefully selected global stations was used to realize the results to ITRF2000. The results in ITRF2000 were then rotated using the ITRF2000 No Net Rotation (NNR) Absolute Rotation Pole for Eurasia. Comparison of their solution with the previous results from *Johansson et al.* [2002] indicated a radial bias between the solutions of ~0.5 mm/yr, which they hypothesized was due to differences in the reference frame realization. Overall, comparisons with the *Johansson et al.* [2002] GPS solution, a GIA model, and results from *Ekman* [1998] lead *Lidberg et al.* [2007] to conclude that their solution has an accuracy in the radial component at the 0.5 mm/yr level and an internal consistency in the horizontal component of 0.2 mm/yr (for the best GPS stations with long observation spans).

3.2. GRACE Data

[26] We estimated rates of change in FAGA using GRACE data from the University of Texas at Austin Center for Space Research (CSR) Release-04 (RL04) (Figure 1c). We also tested rates estimated using the GeoForschungsZentrum Potsdam (GFZ) RL04 data. For both data sets we used data for the period from August 2002 to July 2008. Systematic errors in the data that cause north-south striping were reduced ("destriped") following a similar technique to that described by *Swenson and Wahr* [2006]. The gridded rates were geographically smoothed with a Gaussian filter of 400 km width, and sampled to a 2° grid. This relatively coarse sampling was chosen to avoid having a significant bias in the number of GRACE data points compared to the number of GPS and tide gauge stations. Nearby points on a fine-resolution grid will also be highly correlated. Hydrological effects were removed using the Global Land Data Assimilation Systems (GLDAS) model for water storage [*Rodell et al.*, 2004]. (GLDAS uses ground- and space-based observations to constrain models for land sur-

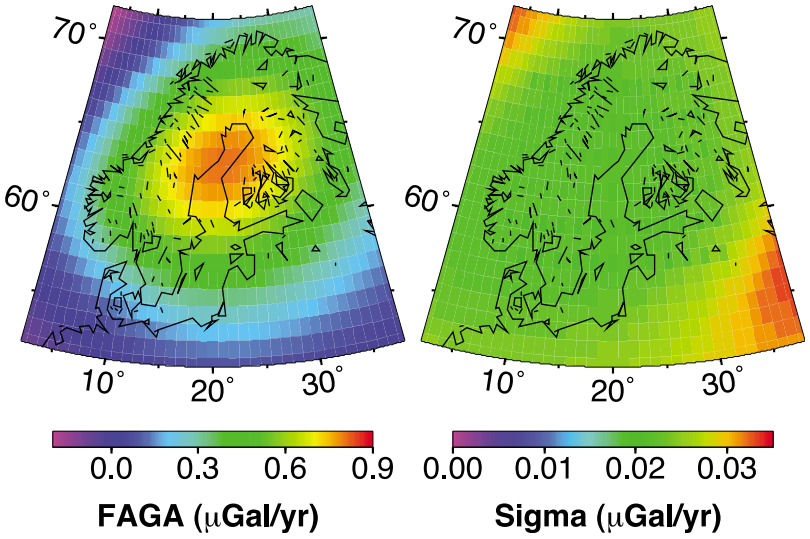

Figure 5. Output model for gravity anomaly, with all geodetic data sets assimilated.

face states. It does not include a groundwater component.) For consistency, the GLDAS data were destriped and smoothed using the same routine as that used for the GRACE data.

3.3. Tide Gauge Data

[27] We estimated rates of RSL change for all tide gauges in the area that have ≥40 years of data (Figure 1d). For these sites we used all available monthly Revised Local Reference (RLR) data, although we also present results for rates calculated only using monthly data between 1950 and 2000. We also, as with the GPS data set, omitted stations along the south coast of the Baltic Sea.

3.4. GIA Models

[28] As described in section 2, the a priori GIA estimates for crustal deformation (Figures 2a and 2b), FAGA (Figure 2c), and RSL (Figure 2d) are the average of multiple forward model predictions of GIA, all calculated using a suite of Earth models and the ICE-5G ice model [*Peltier*, 2004]. (These a priori estimates are $\langle m \rangle$ in equation (3).) The Earth models use a range of upper mantle viscosities of 1–10 × 10^{20} Pa s, lower mantle viscosities of 2–50 × 10^{21} Pa s, and lithospheric thickness of 71, 96, and 120 km. This results in a total of 495 models (N_Ω in equation (3)). For consistency, the input FAGA results were derived from the model geoid predictions using the same smoothing and destriping routines used for the GRACE data.

[29] Covariances between all coordinates on our grid (and all station locations) and for all combinations of parameters were also calculated using our collection of GIA forward models. Figure 3 shows examples of correlations (scaled covariances) plotted relative to a single point and the RSL parameter. This indicates, for example, that radial deformation parameters will have an inverse relationship to RSL within the area of peak GIA signal. Similar plots could be made for all other parameter and coordinate combinations.

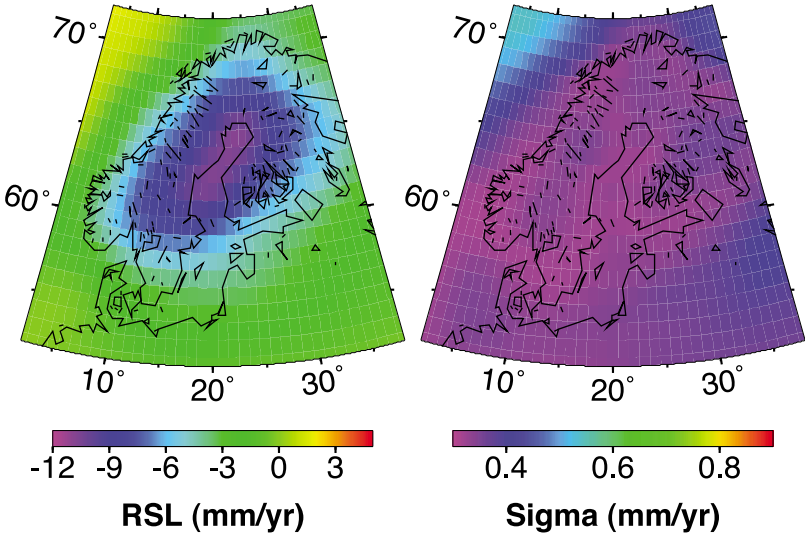

Figure 6. Output model for RSL, with all geodetic data sets assimilated.

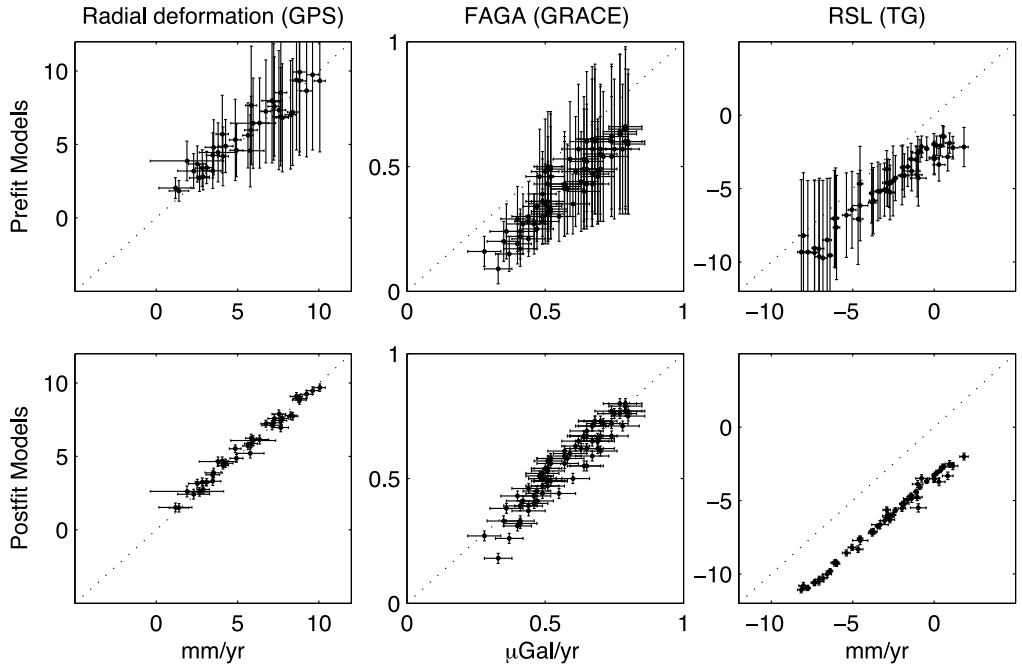

Figure 7. Comparison of a priori and output model results with observations. Regional sea level rise is not included in the models, hence the points for the RSL plots fall off the diagonal. Uncertainties for the a priori predictions are due to the wide range of Earth models used in their calculation.

An adjustment was made to the forward model predictions to account for the fact that across our small study area the horizontal effects are dominated by far-field effects from the Laurentian ice sheet. Thus, prior to the calculation of the covariance matrix, a rotation across the set of GPS sites was calculated and removed from each model prediction. The resulting covariance matrix shows the expected outward motion of the observation sites from the center of the loading.

4. Results

[30] In Figure 4 we show output crustal deformation models obtained after different combinations of geodetic data were assimilated (i.e., if a geodetic data set has been assimilated it was included in the observation vector, d, of equation (1)). Assimilating only the GPS data produces a peak maximum uplift of 9.2 ± 0.5 mm/yr, while assimilating only the tide gauge or GRACE rates slightly increases these rates (maximum uplifts of 10.5 ± 0.5 mm/yr). (Assimilated GRACE rates were estimated from the CSR data set, unless otherwise noted.) Assimilating all the data leads to the greatest peak uplift (11.4 ± 0.3 mm/yr). Peak uplift is located at (23°E, 65°N) for all combinations of observations except GRACE only, which is located at (21°E, 63°N). Including the GPS results reduces the horizontal velocities, particularly to the SE of the Baltic, while including the GRACE data increases these velocities.

[31] We also show the output FAGA model (Figure 5) and RSL model (Figure 6), both with all data assimilated. Figure 7 indicates the much closer agreement of the output models with the observations, compared with the agreement between a priori predications and observations.

[32] Figures 4, 5, and 6 also show estimated sigmas for the models. It is clear from Figure 4 that uncertainties are reduced as more data is assimilated into the model. For example, mean uncertainties are 0.5 mm/yr for a GPS-only

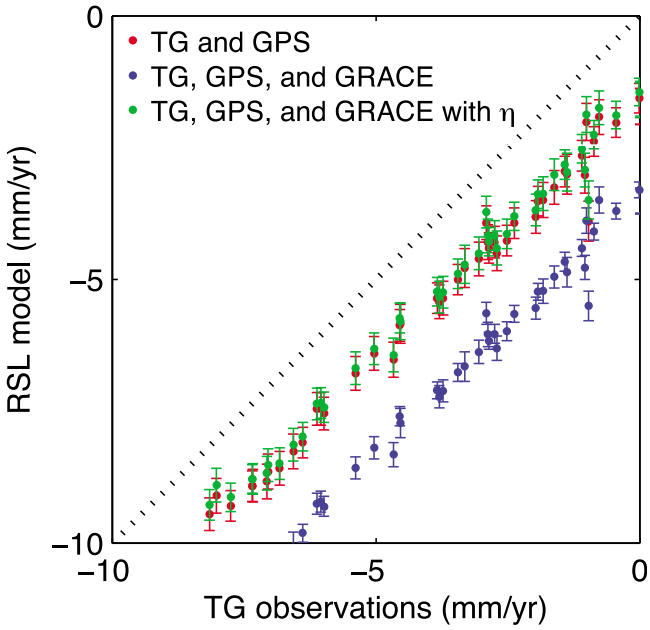

Figure 8. Comparison of output model and observations for RSL, with different geodetic data sets assimilated. The model solution with η included a simultaneous estimation of a uniform regional gravity rate. For clarity the error bars for TG observations are not shown.

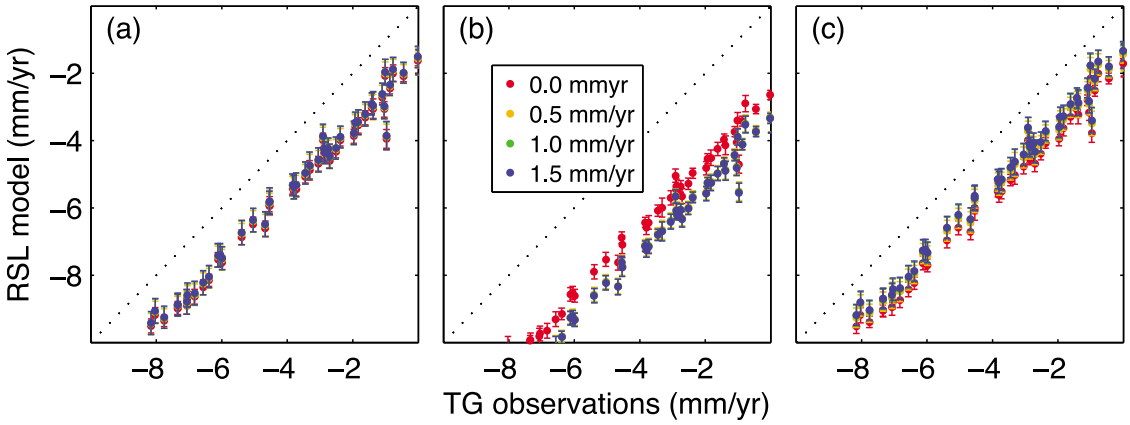

Figure 9. Comparison of output RSL model with tide gauge rates, with different colors indicating different a priori reference frame constraints. (a) No GRACE rates were assimilated into the model (only GPS and tide gauge), (b) GRACE rates were also assimilated, and (c) GRACE rates were also assimilated and a uniform regional gravity rate was estimated.

assimilation, while they are 0.4 mm/yr with all data assimilated. The ability to simultaneously estimate uncertainties in the model is a distinct advantage of using this technique.

5. Regional Sea Level Rate

[33] The estimated value for regional average relative sea level rate ($\dot{\mu}$) varies according to a number of factors. We discuss these factors here. Changes to $\dot{\mu}$ are linked to uniform shifts of the entire GIA solution relative to the data. All sigmas given for $\dot{\mu}$ are the formal standard error output by the assimilation code.

[34] The most significant changes to $\dot{\mu}$ occur when the GRACE data are assimilated. Assimilating the GRACE data significantly increases the estimated value, from 1.6 ± 0.3 mm/yr when only GPS and tide gauge rates are assimilated to 3.3 ± 0.1 mm/yr when GRACE rates are added. Figure 8 shows the shift that causes this change (red versus blue dots).

[35] We experimented with using different levels of constraint on the estimated GPS reference frame parameters. For a solution with only GPS and tide gauge rates assimilated, $\dot{\mu}$ is very similar with and without reference frame parameters constrained to zero (Figure 9a). However, when GRACE rates are included in the assimilation there is a bias between results with a constrained reference frame and those with an a priori reference frame sigma of 0.5 mm/yr ($\dot{\mu}$ = 2.6 ± 0.1 compared to 3.3 ± 0.1 mm/yr). This offset is clearly visible in Figure 9b. Increases in the a priori reference frame sigma beyond 0.5 mm/yr do not lead to a further change in $\dot{\mu}$. (Although the reference frame parameters themselves do change, the effect on the radial GIA field is negligible.)

[36] The tide gauge rates were calculated using all available data for stations with ≥40 years of data. This could cause inconsistencies due to different ocean processes occurring in the different time periods used. We therefore tested an assimilation with rates calculated using only data between 1950 and 2000. This produced (without GRACE data assimilated) an estimate for $\dot{\mu}$ of 1.7 ± 0.3 mm/yr, which is similar to our previous estimate. Use of a considerably smaller data span, however, does result in a significant change to our estimate for $\dot{\mu}$. For example, using only tide gauge data between 1990 and 2000 produces an estimated rate of −1.3 ± 0.7 mm/yr.

[37] Results also vary according to the GRACE parameters used (e.g., spatial sampling resolution, data processing center, or whether we scale the uncertainties). For example, if data from the GFZ processing center are used instead of those from CSR the uplift area is stronger, producing an estimated value for $\dot{\mu}$ of 3.6 ± 0.1 mm/yr (compared to 3.3 ± 0.1 mm/yr for CSR data).

6. Regional Uniform Gravity Rate

[38] Bearing in mind the bias between results produced with and without the GRACE data assimilated (section 5), we decided to experiment with introducing to the model a uniform gravity rate across the Fennoscandia region.

[39] We therefore adjusted the observation equation for the GRACE rates to be

$$\dot{G}_{GRACE}(\lambda,\phi) = \dot{G}_{GIA}(\lambda,\phi) + \dot{\eta} + \varepsilon_{GRACE}(\lambda,\phi) \qquad (14)$$

where $\dot{\eta}$ is a uniform, regional, gravity rate.

[40] Including this rate (estimated at 0.22 ± 0.03 μGal/yr) eliminates much of the bias between solutions with and without the GRACE data included. Peak GIA signal in the output models is considerably reduced compared to models without $\dot{\eta}$ included in the assimilation (9.5 ± 0.4 mm/yr compared to 11.4 ± 0.3 mm/yr, with all data assimilated), since the entire solution is shifted down (Figure 10). This brings the estimate for peak uplift closer to the estimates without the GRACE data assimilated. This also brings the RSL model to a level consistent with that estimated without the GRACE data (Figure 8), so the corresponding estimate for $\dot{\mu}$ (1.4 ± 0.2 mm/yr) is also more consistent. Although our estimate for peak FAGA without $\dot{\eta}$ included (0.8 ± 0.1 μGal/yr) was already lower than the ~1.2 μGal/yr estimated by *Steffen et al.* [2008], to gain consistency in our results the solution seems to require an even lower peak FAGA rate of 0.6 ± 0.1 μGal/yr.

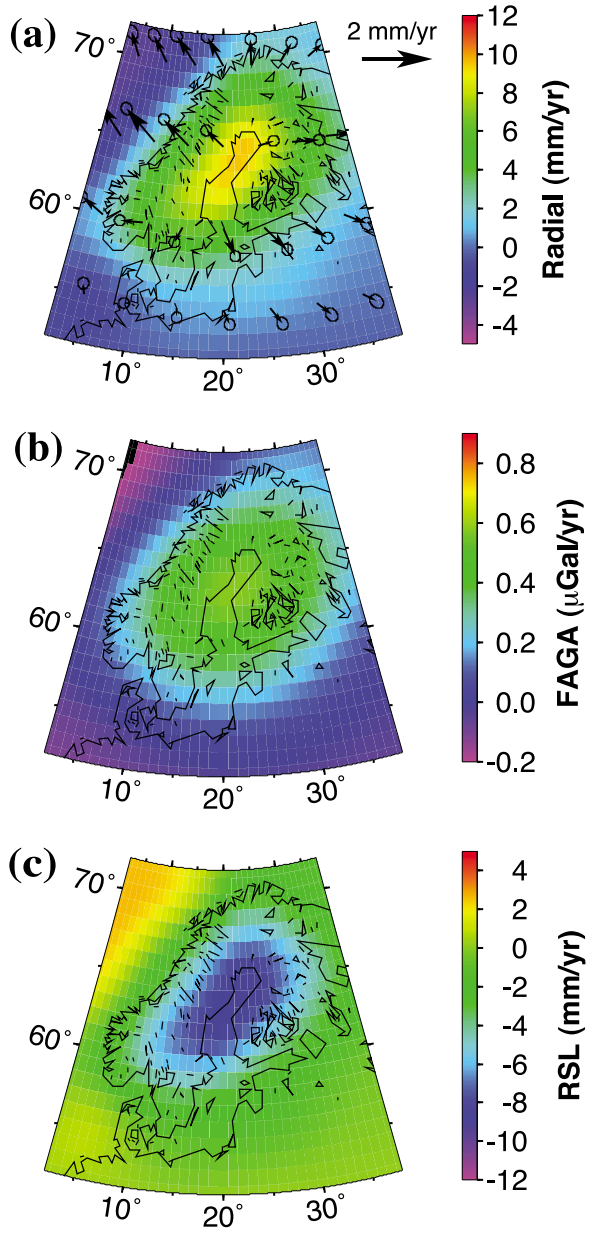

Figure 10. Model results when a uniform, regional, gravity rate is included in the estimation: (a) Horizontal and radial deformation, (b) FAGA, and (c) RSL.

[41] Use of this uniform regional gravity rate also has the effect of reducing the bias seen between results with and without the reference frame parameters constrained (Figure 9c). In fact, inclusion of $\dot{\eta}$ results in reasonable consistency in the model results and estimate for $\dot{\mu}$ regardless of whether the GRACE data is included and regardless of a priori reference frame uncertainties.

[42] Use of GFZ GRACE data results in a different estimate for $\dot{\eta}$ (0.28 ± 0.03 μGal/yr) compared to that for CSR (0.22 ± 0.03 μGal/yr). However, use of this regional gravity rate results in better agreement for estimated values of $\dot{\mu}$ (1.3 ± 0.2 mm/yr for GFZ and 1.4 ± 0.2 mm/yr for CSR, compared with 3.6 ± 0.1 mm/yr for GFZ and 3.3 ± 0.1 mm/yr for CSR without the uniform gravity rate included). Similarly, peak model uplift when the GFZ rates are assimilated is reduced to a more consistent 9.5 ± 0.4 mm/yr (compared with 11.9 ± 0.3 mm/yr without a uniform gravity rate included).

7. Collocated GPS and Tide Gauge Sites

[43] A number of other studies [e.g., *Milne et al.*, 2001; *Johansson et al.*, 2002] have estimated $\dot{\mu}$ using a more direct "correction" of the tide gauge rates using land uplift rates from collocated GPS sites or estimates at the tide gauge locations from a polynomial fit to the GPS rates. A model of the sea surface change is also required. The relationship between these parameters can be expressed as

$$\dot{s}_{TG}(\lambda,\phi) = \dot{g}_{MODEL}(\lambda,\phi) - \dot{r}_{GPS}(\lambda,\phi) + \dot{\mu} \qquad (15)$$

where $\dot{s}_{TG}(\lambda,\phi)$ is an estimated tide gauge rate, $\dot{g}_{MODEL}(\lambda,\phi)$ is an estimate of the sea surface rate from a model, $\dot{r}_{GPS}(\lambda,\phi)$ is estimated radial deformation rate from GPS, and $\dot{\mu}$ is uniform sea level rate.

[44] We carried out a similar study using the tide gauge and GPS rates used for our assimilation calculations. We selected collocated sites based on the condition that a GPS station must be within 1° of a tide gauge. If there was more than one tide gauge within the 1° we used the closest site. Occasionally a particular GPS station is collocated with several different tide gauges. For the sea surface model we used a forward model that was calculated using a lithospheric thickness of 120 km, upper mantle viscosity of 8×10^{20} Pa s and lower mantle viscosity of 10^{22} Pa s (these are the values for the best fit Earth model estimated by *Milne et al.* [2001]).

[45] Using this technique we estimate a value for $\dot{\mu}$ of 1.7 ± 0.1 mm/yr (Figure 11a). A comparable value (1.6 ± 0.3 mm/yr) is estimated using our assimilation technique, both when only the collocated GPS and tide gauge sites are assimilated (Figure 11b), or when all tide gauge and GPS sites are assimilated (Figure 11c). The results for an assimilation of all the data, including GRACE, are also consistent if the additional $\dot{\eta}$ parameter is estimated. (The smaller uncertainties for the collocation results do not indicate a higher degree of certainty in this rate: The given uncertainties are formal errors estimated using our least squares fit or the assimilation code, and the assimilation code propagates the uncertainties for all a priori predictions and data uncertainties, compared to just GPS and tide gauge rate uncertainties for the collocation study.) Our estimates for $\dot{\mu}$ compare with an estimate of 1.9 ± 0.2 mm/yr from *Johansson et al.* [2002] and 2.1 ± 0.3 mm/yr from *Milne et al.* [2001].

8. Discussion and Conclusions

[46] We successfully assimilate GPS, tide gauge, and GRACE gravity rates into a self-consistent model for GIA in the Fennoscandia region. Our assimilation simultaneously estimates uncertainties, which are decreased as increasing amounts of data are assimilated. The technique mitigates the problem of any inaccuracies in the GPS reference frame by simultaneously estimating reference frame adjustments.

[47] The geographical distribution of our updated GIA models are relatively consistent with previous results. For example, we observe the approximately southwest to

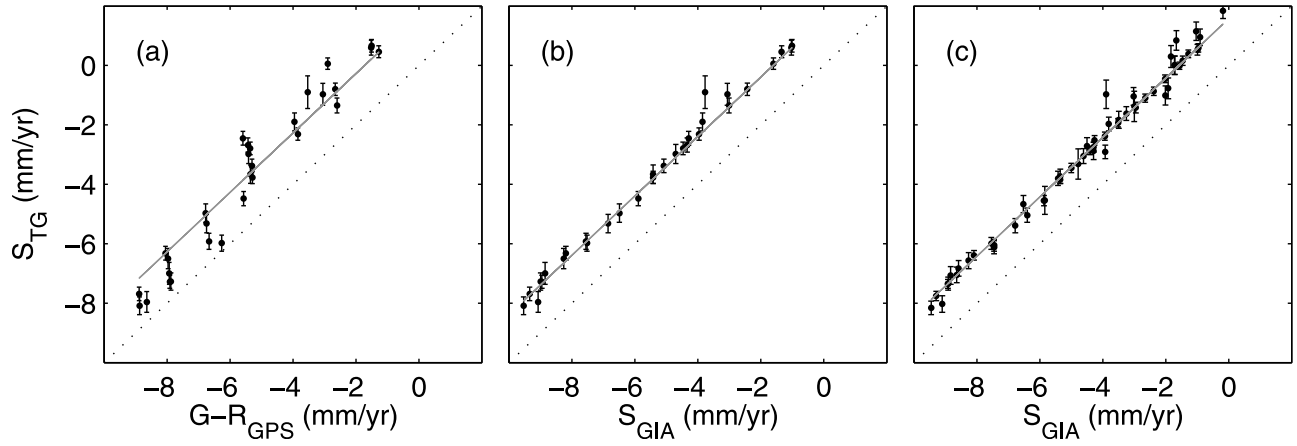

Figure 11. Comparison of RSL rates using (a) collocated GPS and tide gauges and the model described in equation (5), (b) model output from an assimilation using only collocated sites, (c) model output using all available sites.

northeast elongation observed in many other studies. Our final estimate for peak uplift (9.5 ± 0.4 mm/yr) is also consistent with that estimated by previous studies (~10 mm/yr [*Milne et al.*, 2001; *Johansson et al.*, 2002; *Milne et al.*, 2004]). However, our final models indicate a location for peak uplift that is several degrees to the east of many previously published results. Previous model results have generally indicated an area of peak uplift slightly to the west of the northern Gulf of Bothnia [e.g., *Lambeck et al.*, 1998; *Milne et al.*, 2001; *Johansson et al.*, 2002], while our updated model places this location in the middle of the northern Gulf of Bothnia. One explanation for this shift could be the impact of having continuous gridded data (i.e., the distribution of ground observations could bias the estimated location). *Milne et al.* [2001] illustrate the effect of spatial sampling by calculating a polynomial fit to their numerical model values at BIFROST station locations only. The initial model has a larger peak that covers the northern Gulf of Bothnia, while the resampled model has a smaller peak to the west. Our model is also more consistent with the Gaussian fit to BIFROST results illustrated by *Johansson et al.* [2002], who observe peak uplift from their observations several degrees east of peak uplift for their best fit model. Perhaps the observations, which are reflected in our model, are indicating that the ice models used may not accurately reflect the true ice thickness for the area.

[48] Our estimates for a regional relative sea level rate (~1.5 mm/yr) are consistent regardless of a priori reference frame uncertainties or which combination of data sets are assimilated, although if GRACE data are included this is only the case if a uniform regional gravity rate is also estimated. Our estimates for sea level rate are also relatively consistent with previously published values.

[49] There are several possible explanations for the requirement of a uniform regional gravity rate to assimilate the GRACE data with consistent results. Any far-field contributions to the GRACE gravity field that are unmodeled by our regional GIA field will appear as a nearly geographically constant offset in our solution. Such contributions may be due to an error in the low-order harmonics of the GRACE field, or simply an effect that is not associated with GIA. It is possible, for example, that errors in the model estimates of GIA for the Laurentia ice sheet over North America (the effects of which are included in our a priori GIA predictions and covariances) cause a bias across Fennoscandia that appears uniform due to the small size of the region.

[50] Alternatively, *Steffen et al.* [2008] note that secular variations in the GRACE data may be affected by aliasing errors associated with mismodeling of the ocean tides, particularly at high latitudes such as this. *Ray et al.* [2003] showed that aliasing of K1 and K2 tides could cause interannual signals in the GRACE data with 7.4 and 3.7 year periods, which will cause inaccuracies in our estimation of the gravity rate for our relatively short (6 year) data span. In future work we should include estimated cycles at these periods in our rate calculations. Similarly, inconsistencies could be caused by the relatively short time period sampled by the GRACE data. We indicated through comparison of estimated sea level rates for different time periods that longer-period (e.g., decadal) changes in sea level can be significant. Other possibilities are mismodeling of the hydrology signal over Fennoscandia (*Steffen et al.* [2008] show that other hydrological models have quite different patterns, and also suggest that some very long period hydrological trends could exist that would affect our rate estimates) or inconsistencies caused by our application of the GRACE destriping or smoothing routine to both model and data. This new technique provides an excellent platform for exploring these questions further.

Appendix A: Matrix Identities Used

[51] Here we state without proof the matrix identities used at the end of section 2.1:

$$PB^T\left(BPB^T+R\right)^{-1}=\left(B^TR^{-1}B+P^{-1}\right)^{-1}B^TR^{-1} \tag{A1}$$

$$P-PB^T\left(BPB^T+R\right)^{-1}BP=\left(B^TR^{-1}B+P^{-1}\right)^{-1} \tag{A2}$$

where P and R are positive definite matrices. Equation (A2) is known as the Woodbury identity [*Golub and van Loan*, 1996]. The identities are derived by inverting via block elimination a 2 × 2 block matrix. The elimination is per-

formed first in one direction and then the other, and the two results are equated.

[52] **Acknowledgments.** This work was supported by NASA grants NNX08AJ79G and NNX07AM77G (EMH and JLD), and by the Natural Environment Research Council's Oceans 2025 program (MET). We thank R. Hass for useful discussions regarding least squares collocation, and are grateful to K. Fleming and R. Sabadini for their insightful reviews. This work also benefitted from discussions with members of the Stable North America Reference Frame (SNARF) Working Group. Some figures were generated using the Generic Mapping Tools [*Wessel and Smith*, 1998].

References

Bennett, A. F. (2002), *Inverse Modeling of the Ocean and Atmosphere*, 234 pp., Cambridge Univ. Press, Cambridge, U. K.

Bills, B. G., and T. S. James (1996), Late quaternary variations in relative sea level due to glacial cycle polar wander, *Geophys. Res. Lett.*, *23*, 3023–3026, doi:10.1029/96GL02886.

Clark, J. A., W. E. Farrell, and W. R. Peltier (1978), Global changes in postglacial sea level: A numerical calculation, *Quat. Res.*, *9*, 265–287.

Davis, J. L., J. X. Mitrovica, H.-G. Scherneck, and H. Fan (1999), Investigations of Fennoscandian glacial isostatic adjustment using modern sea level records, *J. Geophys. Res.*, *104*, 2733–2747, doi:10.1029/1998JB900057.

Ekman, M. (1998), Postglacial uplift rates for reducing vertical positions in geodetic reference systems, in *Proceedings of the General Assembly of the Nordic Geodetic Commission*, edited by B. Jonsson, pp. 401–407, Landmäteriet, Gävle, Sweden.

Farrell, W. E., and J. A. Clark (1976), On postglacial sea level, *Geophys. J. R. Astron. Soc.*, *46*, 647–667.

Golub, G. H., and C. F. van Loan (1996), *Matrix Computations*, 3rd ed., 694 pp., Johns Hopkins Univ. Press, Baltimore, Md.

Han, D., and J. Wahr (1989), Post-glacial rebound analysis for a rotating Earth, in *Slow Deformations and Transmission of Stress in the Earth*, *Geophys. Monogr. Ser.*, vol. 49, edited by S. Cohen and P. Vanicek, pp. 1–6, AGU, Washington, D. C.

Johansson, J. M., et al. (2002), Continuous GPS measurements of postglacial adjustment in Fennoscandia: 1. Geodetic results, *J. Geophys. Res.*, *107*(B8), 2157, doi:10.1029/2001JB000400.

Johnston, P. (1993), The effect of spatially non-uniform water loads on predictions of sea level change, *Geophys. J. Int.*, *114*, 615–634.

Kendall, R. A., J. X. Mitrovica, and G. A. Milne (2005), On post-glacial sea level – II. Numerical formulation and comparative results on spherically symmetric models, *Geophys. J. Int.*, *161*, 679–706.

Kuo, C. Y., C. K. Shum, A. Braun, and J. X. Mitrovica (2004), Vertical crustal motion determined by satellite altimetry and tide gauge data in Fennoscandia, *Geophys. Res. Lett.*, *31*, L01608, doi:10.1029/2003GL019106.

Lambeck, K., C. Smither, and M. Ekman (1998), Tests of glacial rebound models for Fennoscandia based on instrumented sea- and lake-level records, *Geophys. J. Int.*, *135*, 375–387.

Latychev, K., J. X. Mitrovica, J. Tromp, M. E. Tamisiea, D. Komatistsch, and C. C. Christara (2005), Glacial isostatic adjustment on 3-D Earth models: A finite-volume formulation, *Geophys. J. Int.*, *159*, 421–444.

Lidberg, M., J. M. Johansson, H.-G. Scherneck, and J. L. Davis (2007), An improved and extended GPS-derived 3D velocity field of the glacial isostatic adjustment (GIA) in Fennoscandia, *J. Geod.*, *81*, 213–230, doi:10.1007/s00190-006-0102-4.

Marotta, A. M., J. X. Mitrovica, R. Sabadini, and G. Milne (2004), Combined effects of tectonics and glacial isostatic adjustment on intraplate deformation in central and northern europe: Applications to geodetic baseline analyses, *J. Geophys. Res.*, *109*, B01413, doi:10.1029/2002JB002337.

Martinec, Z. (2000), Spectral-finite element approach to three-dimensional viscoelastic relaxation in a spherical earth, *Geophys. J. Int.*, *142*, 117–141.

Milne, G., and J. Mitrovica (1996), Postglacial sea level change on a rotating Earth; first results from a gravitationally self-consistent sea level equation, *Geophys. J. Int.*, *126*, F13–F20.

Milne, G., J. Mitrovica, and J. L. Davis (1999), Near-field hydro-isostasy: The implementation of a revised sea-level equation, *Geophys. J. Int.*, *139*, 464–482.

Milne, G. A., J. L. Davis, J. X. Mitrovica, H.-G. Scherneck, J. M. Johansson, M. Vermeer, and H. Koivula (2001), Space-geodetic constraints on glacial isostatic adjustment in Fennoscandia, *Science*, *291*, 2380–2385.

Milne, G. A., J. X. Mitrovica, H.-G. Scherneck, J. L. Davis, J. M. Johansson, H. Koivula, and M. Vermeer (2004), Continuous GPS measurements of postglacial adjustment in Fennoscandia, 2. Modeling results, *J. Geophys. Res.*, *109*, B02412, doi:10.1029/2003JB002619.

Mitrovica, J. X., and G. A. Milne (2003), On post-glacial sea level I: General theory, *Geophys. J. Int.*, *154*, 253–267.

Mitrovica, J. X., and W. R. Peltier (1991), On postglacial geoid subsidence over the equatorial oceans, *J. Geophys. Res.*, *96*, 20,053–20,071, doi:10.1029/91JB01284.

Mitrovica, J. X., M. E. Tamisiea, J. L. Davis, and G. A. Milne (2001), Recent mass balance of polar ice sheets inferred from patterns of global sea level change, *Nature*, *409*, 1026–1029.

Mitrovica, J. X., J. Wahr, I. Matsuyama, and A. Paulson (2005), The rotational stability of an ice-age earth, *Geophys. J. Int.*, *161*, 491–506, doi:10.1111/j.1365-246X.2005.02609.x.

Moritz, H. (1980), *Advanced Physical Geodesy*, H. Wichmann, Karlsruhe, Germany.

Paulson, A., S. Zhong, and J. Wahr (2005), Modelling post-glacial rebound with lateral viscosity variations, *Geophys. J. Int.*, *163*, 357–371, doi:10.1111/j.1365-246X.2005.02645.x.

Peltier, W. R. (1974), The impulse response of a Maxwell Earth, *Rev. Geophys.*, *12*, 649–669.

Peltier, W. R. (1994), Ice-age paleotopography, *Science*, *265*, 195–201.

Peltier, W. R. (1998), "Implicit ice" in the global theory of glacial isostatic adjustment, *Geophys. Res. Lett.*, *25*, 3955–3958, doi:10.1029/1998GL900076.

Peltier, W. R. (2004), Global glacial isostacy and the surface of the ice-age Earth: The ICE-5G (VM2) model and GRACE, *Ann. Res. Earth Planet. Sci.*, *32*, 111–149.

Ray, R. D., D. D. Rowlands, and G. D. Egbert (2003), Tidal models in a new era of satellite gravimetry, *Space Sci. Rev.*, *108*, 271–282.

Rodell, M., et al. (2004), The Global Land Data Assimilation System, *Bull. Am. Meteorol. Soc.*, *85*, 381–394.

Sabadini, R., and B. Vermeersen (2004), *Global Dynamics of the Earth: Applications of Normal Mode Relaxation Theory to Solid-Earth Geophysics*, 328 pp., Kluwer Acad. Publ., Dordrecht, Netherlands.

Steffen, H., H. Denker, and J. Müller (2008), Glacial isostatic adjustment in Fennoscandia from GRACE data and comparison with geodynamical models, *J. Geodyn.*, *46*, 155–164.

Swenson, S., and J. Wahr (2006), Post-processing removal of correlated errors in GRACE data, *Geophys. Res. Lett.*, *33*, L08402, doi:10.1029/2005GL025285.

Tamisiea, M. E., J. X. Mitrovica, G. A. Milne, and J. L. Davis (2001), Global geoid and sea level changes due to present-day ice mass fluctuations, *J. Geophys. Res.*, *106*, 30,849–30,864, doi:10.1029/2000JB000011.

Tromp, J., and J. X. Mitrovica (2000), Surface loading of a viscoelastic Earth—III. Aspherical models, *Geophys. J. Int.*, *140*, 425–441.

Wahr, J., and J. L. Davis (2002), Geodetic constraints on glacial isostatic rebound, in *Glacial Isostatic Adjustment and the Earth System*, *Geodyn. Ser.*, vol. 29, edited by J. X. Mitrovica and L. L. A. Vermeersen, pp. 3–32, AGU, Washington, D. C.

Wessel, P., and W. H. F. Smith (1998), New improved version of the Generic Mapping Tools released, *Eos Trans. AGU*, *79*, 579, doi:10.1029/98EO00426.

Woodworth, P. L., and R. Player (2003), The Permanent Service for Mean Sea Level: An update to the 21st century, *J. Coastal Res.*, *19*, 287–295.

Wu, P. (2004), Using commercial finite element packages for the study of earth deformations, sea levels and the state of stress, *Geophys. J. Int.*, *158*, 401–408.

Xu, G. (2003), *GPS: Theory, Algorithms, and Applications*, 315 pp., Springer, New York.

J. L. Davis and E. M. Hill, Harvard-Smithsonian Center for Astrophysics, 60 Garden St., MS 42, Cambridge, MA 02138, USA. (jdavis@cfa.harvard.edu; ehill@cfa.harvard.edu)

M. Lidberg, Geodesy Division, Lantmäteriet, Lantmäterigatan 2, SE-801 82 Gävle, Sweden. (martin.lidberg@lm.se)

M. E. Tamisiea, National Oceanography Centre, Joseph Proudman Building, 6 Brownlow St., Liverpool, L3 5DA, UK. (mtam@pol.ac.uk)